Numerical Modeling of Mantle Flow beneath Madagascar to Constrain Upper Mantle Rheology Beneath Continental Regions

T.A. Rajaonarison[1], D.S. Stamps[1], S. Fishwick[2], S. Brune[3,4], A. Glerum[3], J. Hu[5]

[1]Virginia Tech

[2]University of Leicester

[3]GFZ German Research Center of Geosciences

[4]University of Potsdam

[5]California Institute of Technology

Introduction

The content of the supporting information includes (1) test results (Figure S1) of SKS splitting parameter calculations for an anisotropic layer ∼125-200 km for the Edge-Driven Convection (EDC) model, (2) descriptions of 6 spreadsheets of model outputs that are available in the PANGAEA repository with doi:10.1594/PANGAEA.909406, (3) Figure S2, S3 show the calculated mantle flow fields for the lithosphere-mantle wind models for Behn et al. (2004) and Forte et al. (2010), and (4) Figure S4,S5 showing calculated TI axis derived lithosphere-mantle wind interactions models for Behn et al. (2004) and Forte et al. (2010).

Synthetic splitting derived from the Edge-Driven Convection model for an ∼125-200 km anisotropic layer

For the EDC model, we calculate synthetic splitting parameters by considering ∼125-200 km anisotropic layer and setting aggregates at shallow and deeper depths to isotropic. The aim of this test is to investigate whether the single anisotropic layer from ∼125-200 km reproduces similar delay times as the entire ∼100-400 km, which would suggest a single layer anisotropy model.

Figure S1 shows the comparison of the synthetic splitting and the observations. In northern Madagascar (Region A; Figure S1) the predicted splitting aligns well with the observations pattern (18° misfit). We found relatively large mean misfit 36° in central Madagascar (Region B; Figure S1). In southern Madagascar (Region C and D; Figure S1), the mean misfits are 24° and 26° for south-central and southeastern Madagascar, respectively. The average delay times are $0.78s$, $0.71s$, $0.67s$ and $0.70s$ for northern, central, south-central and southeastern Madagascar, respectively. This result suggest that considering the EDC reproduce well the observations when the ∼125-200 km anisotropic layer with a slightly lower delay times that the observations. This demonstrate that the most of the anisotropy are mostly sourced from ∼125-200 km where dislocation creep regime dominates.

Additional Supporting Information

The model outputs from this study are available in the PANGAEA repository with doi:10.1594/PANGAEA.909406. The model outputs are in the following spreadsheets:

1. model1_splitting_parameters.xlsx

Calculated splitting parameters derived from Edge-Driven Convection (EDC) model at individual stations formatted as: Stations name, longitude [°], latitude[°], calculated fast azimuth ϕ_{calc}[°], calculated fast azimuth standard deviation [°], and delay time δt [sec].

2. model2_splitting_parameters.xlsx

Calculated splitting parameters derived from the lithosphere-mantle wind model of Behn et al. (2004) at individual stations formatted as: Stations name, longitude [°], latitude[°], calculated fast azimuth ϕ_{calc}[°], calculated fast azimuth standard deviation [°], and delay time δt [sec].

3. model3_splitting_parameters.xlsx

Calculated splitting parameters derived from the lithosphere-mantle wind model of Forte et al. (2010) at individual stations formatted as: Stations name, longitude [°], latitude[°], calculated fast azimuth ϕ_{calc}[°], calculated fast azimuth standard deviation [°], and delay time δt [sec].

4. model1_TI_axis.xlsx

Calculated EDC-derived TI axis at individual seismic stations and at regular grids of $0.5° \times 0.5°$. The file is formatted as longitude [°], latitude[°], depth [km], azimuth [°], and percentage anisotropy [%].

5. model2_TI_axis.xlsx

Calculated TI axis derived from the lithosphere-mantle wind model of Behn et al., (2004) at individual seismic stations and at regular grids of $0.5^\circ \times 0.5^\circ$. The file is formatted as longitude [°], latitude[°], depth [km], azimuth [°] ,and percentage anisotropy [%].

6. model3_TI_axis.xlsx

Calculated TI axis derived from the lithosphere-mantle wind model of Forte et al., (2010) at individual seismic stations and at regular grids of $0.5^\circ \times 0.5^\circ$. The file is formatted as longitude [°], latitude[°], depth [km], azimuth [°], and percentage anisotropy [%].

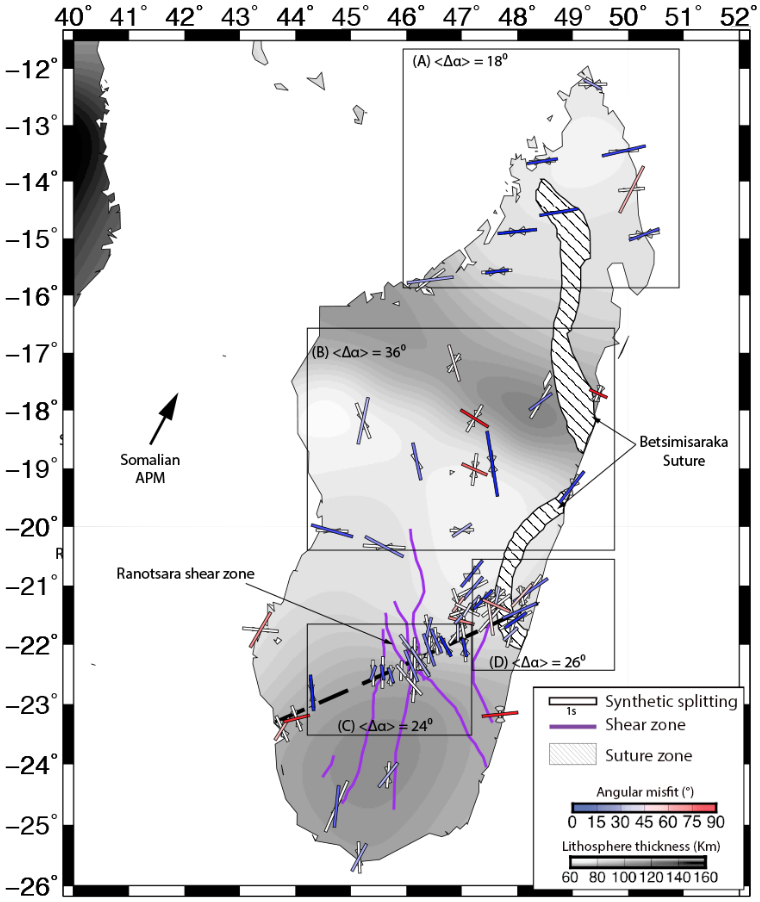

Figure S1. Comparison of synthetic splitting directions derived from EDC (white bars) with SKS splitting measurement bars colored according to angular misfit [0° - 90°] (Reiss et al., 2016; Ramirez et al., 2018). Gray wedges represent confidence interval associated with the synthetic splitting. Rectangular boxes A,B,C, and D depict key regions and $<\Delta\alpha>$ indicates regional circular mean angular misfit within each rectangular box. Purple lines show shear zones after Martela et al. (2000). Background gray scale color shows lithospheric thickness, an updated version of Fishwick (2010). The black dashed line indicates the SELASOMA profile. Black arrows show the Somalian plate Absolute Plate Motion (Argus et al., 2010).

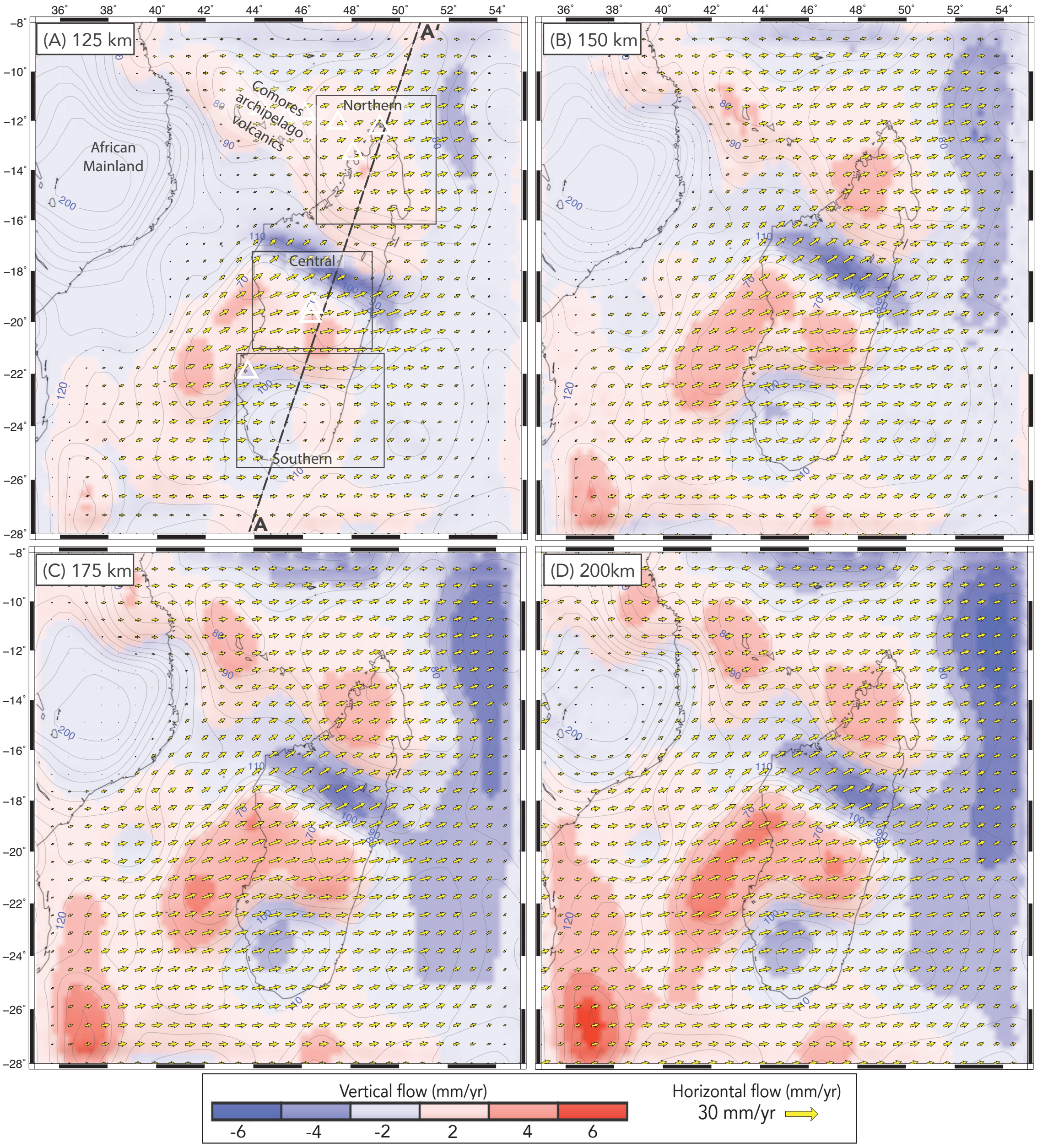

Figure S2. Depth slices showing lithosphere-mantle wind interactions from Behn et al. (2004) global mantle flow with EDC beneath Madagascar at (A) 125 km, (B) 150 km, (C) 175 km, and (D) 200 km depths at initial time (Time = 0 Ma). Background color indicates vertical flow. Yellow vectors portray horizontal flow. We infer two regions below Madagascar that are dominated by upwelling and two regions with downwelling. White triangles in (A) indicate Cenozoic volcanic regions.

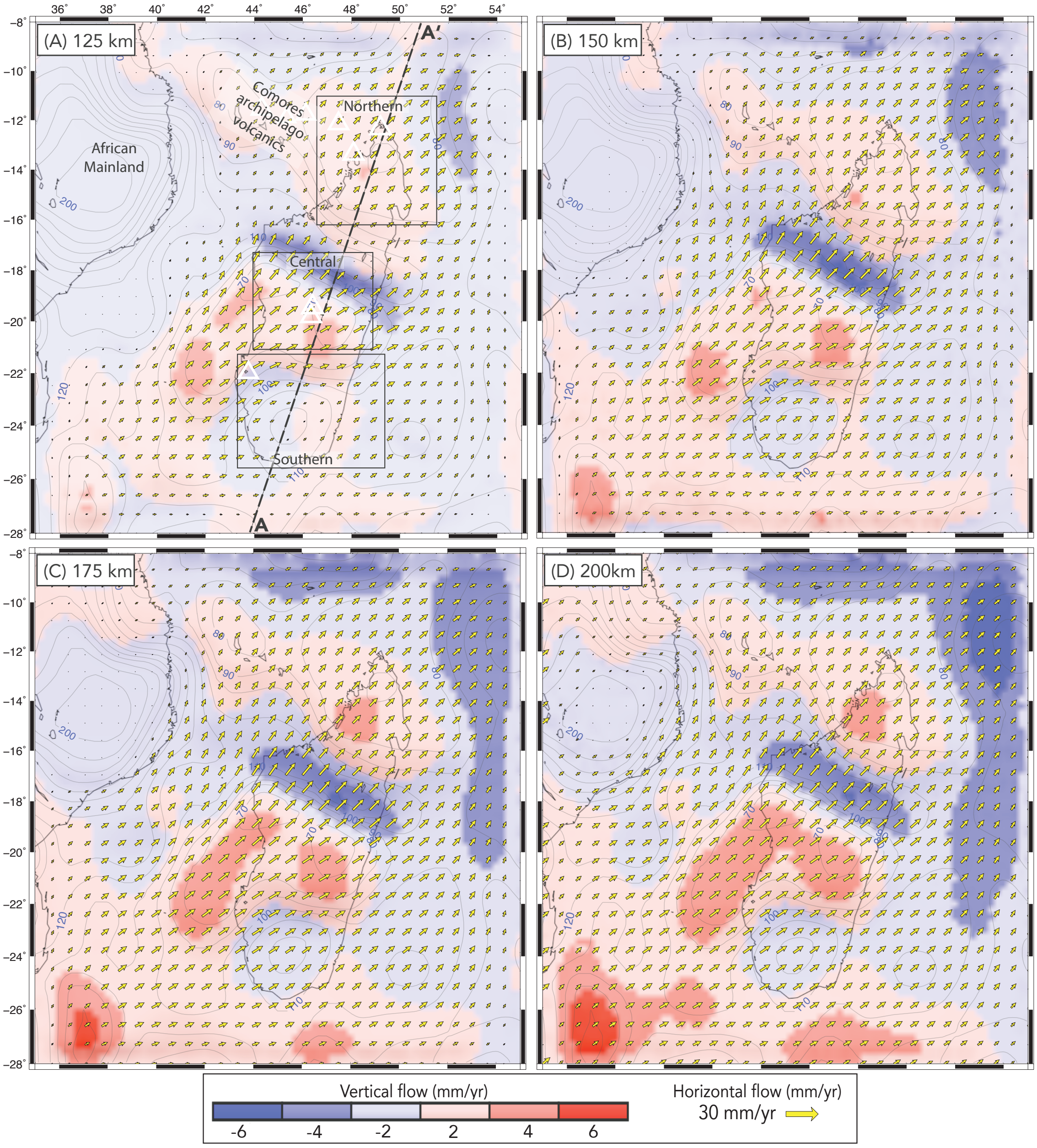

Figure S3. Depth slices showing lithosphere-mantle wind interactions from Forte et al. (2010) global mantle flow with EDC beneath Madagascar at (A) 125 km, (B) 150 km, (C) 175 km, and (D) 200 km depths at initial time (Time = 0 Ma). Background color indicates vertical flow. Yellow vectors portray horizontal flow. We infer two regions below Madagascar that are dominated by upwelling and two regions with downwelling. White triangles in (A) indicate Cenozoic volcanic regions.

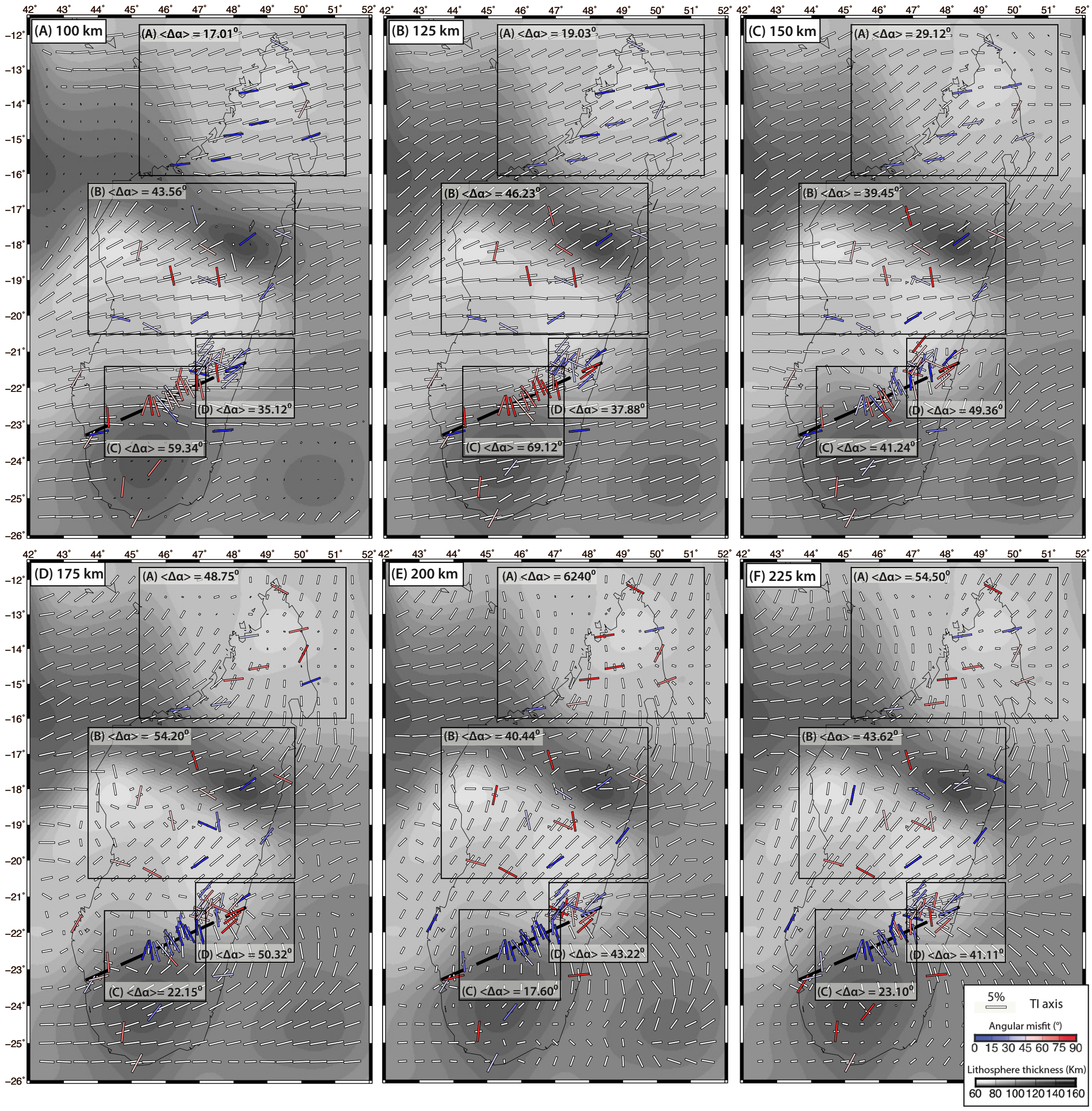

Figure S4. Comparison of TI axis derived from mantle wind from Behn et al. (2004) interactions and observed SKS splitting (Ramirez et al., 2018; Reiss et al., 2016) at depth of (A) 100 km, (B) 125 km (C) 150 km,(D) 175 km, (E) 200 km and (F) 225 km. The SKS splitting measurement bars are colored according to angular misfit [0° - 90°] . The background shows lithospheric thickness from updated Fishwick (2010). The model output files are available at the PANGAEA repository with doi:10.1594/PANGAEA.909406.

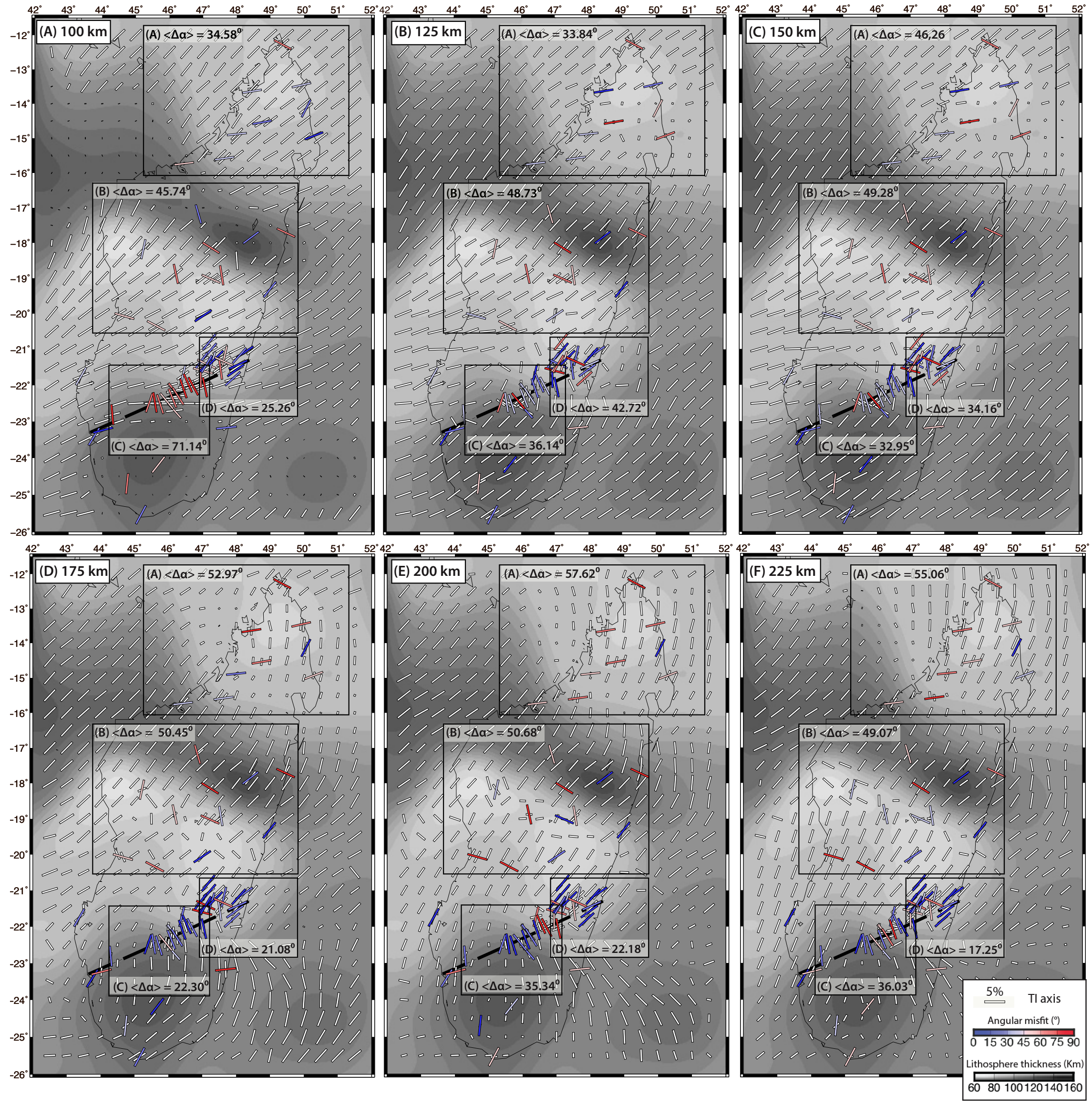

Figure S5. Comparison of TI axis derived from mantle wind from Forte et al. (2010) interactions and observed SKS splitting (Ramirez et al., 2018; Reiss et al., 2016) at depth of (A) 100 km, (B) 125 km (C) 150 km,(D) 175 km, (E) 200 km and (F) 225 km. The SKS splitting measurement bars are colored according to angular misfit [0° - 90°] . The background shows lithospheric thickness from updated Fishwick (2010). The model output files are available at the PANGAEA repository with doi:10.1594/PANGAEA.909406.

References

Behn, M. D., C. P. Conrad, and P. G. Silver (2004), Detection of upper mantle flow associated with the African Superplume,Earth and Planetary Science Letters,224(3-4), 259?274.

Forte, A. M., S. Quéré, R. Moucha, N. A. Simmons, S. P. Grand, J. X. Mitrovica, and D. B. Rowley (2010), Joint seismic?geodynamic-mineral physical modelling of african768geodynamics: A reconciliation of deep-mantle convection with surface geophysical constraints, Earth and Planetary Science Letters,295(3-4), 329?341.

Ramirez, C., A. Nyblade, M. E. Wysession, M. Pratt, F. Andriampenomanana, and 713 T. Rakotondraibe (2018), Complex seismic anisotropy in madagascar revealed by shear 714 wave splitting measurements, Geophysical Journal International, 215(3), 1718?1727.

Reiss, M., G. Rümpker, F. Tilmann, X. Yuan, J. Giese, and E. Rindraharisaona (2016), 719 Seismic anisotropy of the lithosphere and asthenosphere beneath southern Madagascar 720 from teleseismic shear wave splitting analysis and waveform modeling, Journal of Geo721 physical Research: Solid Earth, 121(9), 6627?6643.